Block Transmitted Reference Pulse Cluster Transmission for Terahertz Communications

Lehung Nguyen
Dept. Electrical and Computer Engineering
University of Victoria, Canada
Graduate Student Member, IEEE
Email: nlhung279@uvic.ca

Xiaodai Dong
Dept. Electrical and Computer Engineering
University of Victoria, Canada
Senior Member, IEEE
Email: xdong@ece.uvic.ca

***Abstract*—Terahertz (THz) band (0.1-10 THz) communications is an important technology to meet the demands of the next generation 6G wireless network. The transmitted reference pulse cluster (TRPC) waveform, proposed for ultra-wideband communications, is a suitable candidate for THz communications due to its ultra-broad bandwidth, simple architecture, and built-in robustness to phase noise. In this paper, we achieve a higher data rate for TRPC by proposing a block transmission structure. The prefix before a block is used to address inter-block interference (IBI), and minimum mean-square error (MMSE) based channel estimation and equalization are developed to deal with inter-symbol interference (ISI) arising from high transmission data rates. The performance of the proposed algorithms is verified in the diffuse scattering rich THz channels. Simulation results demonstrate the effectiveness of the proposed algorithms in reducing the influences of IBI and ISI.**

***Index Terms*—6G, THz communications, waveform design, TRPC, channel estimation, channel equalization.**

I. Introduction

THz and sub-THz band (0.1-10 THz) is a critical segment of spectrum to support future 6G wireless systems, considering the availability of bandwidth resources ranging from tens to hundreds of gigahertz, pico-second level symbol duration, integration of thousands of submillimeter-long antennas, and weak interference without full legacy regulation [1]. The impulse radio ultra-wideband (IR-UWB) technology, utilizes both coherent (CR) and non-coherent receiver (NCR) designs [2], is attracting increasing attention for applications in wireless personal area networks (WPANs), wireless sensor networks (WSNs), and the internet of things (IoT), thanks to its low power consumption and the large bandwidth [3]. Transmitted reference pulse cluster (TRPC) [4] is a novel waveform proposed for NCR UWB communications [5]. The TRPC waveform employs a set of pulses in closely-spaced uniform intervals with information encoded in the relative phase of the adjacent sub-pulses. This design facilitates the implementation of a simple, energy-efficient, and resilient autocorrelation detector in the receiver. Moreover, the autocorrelation detector is robust against pulse shape distortion during transmission. The authors in [6] enhance the performance of TR receivers by improving their SNR. Weighted energy receivers (WERs) have also been introduced to improve receiver performance in UWB communications [7]. In [8], the performance of a conventional transmitted-reference (TR) receiver is evaluated using a frequency-shifted reference pulse in a UWB system. In [9], the authors discuss a hybrid pulse position modulation (PPM) and binary phase-shift keying (BPSK) for TRPC structure to increase energy efficiency and data rate. In [10], a practical passband TRPC-based UWB system has been developed and examined to address carrier frequency offset and phase noise that naturally occur in voltage-controlled oscillators (VCO) of both the transmitter and receiver. Recently, a solution to the non-ideal delay line problem in TRPC for UWB communications is introduced in [11]. In [12], an energy-efficient on-off keying TRPC system for UWB communications is proposed. In [13], the authors discuss an energy-efficient weighting strategy for various TRPC-UWB communication systems. In [14], a joint symbol and ToA estimation for iterative TRPC-UWB systems is introduced.

In contrast to lower carrier frequency channels, diffuse scattering from reflective surfaces is a prominent phenomenon at THz frequencies because of surface roughness comparable to the wavelength. This leads to a cluster of dense rays from one reflection surface [15]. Moreover, molecular absorption and frequency-dependent path loss result in limited multipaths from the surroundings, where signals from longer propagation paths will be attenuated substantially. The ultra-narrow pulses of TRPC waveform utilize the ultra-broad bandwidth of the terahertz band that naturally achieves high-resolution multipath discrimination. In addition, TRPC offers a simple transceiver design that avoids full channel state information estimation, which is challenging in THz channels with dense diffuse scattering [16].

One shortcoming of the original TRPC is the limited data rate constrained by the delay spread of the wireless channel, in order to avoid inter-symbol interference (ISI). Inspired by the block transmission and frequency domain equation in coherent communications, this paper proposes a block structure of TRPC, with the objective to increase the date rate. The key idea is to create a block of TRPC symbols, with a symbol duration shorter than the channel delay spread, and a guard interval in front of the block formed by either a zero prefix (ZP) or a cyclic prefix (CP). At the receiver side, minimum mean squared error (MMSE) based block algorithms

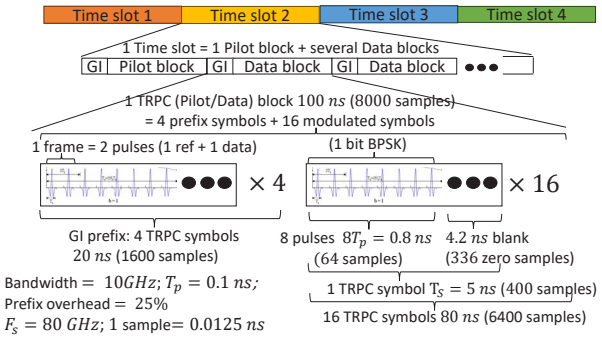

Fig. 1. TDMA for a TRPC Block Transmission example with system bandwidth of 10 GHz, pulse duration $T_p = 0.1$ ns, consisting of 16 modulated symbols and a prefix overhead of 25%. Symbol duration $T_s = 5$ ns, which is equivalent to 400 samples given $F_s = 80$ GHz.

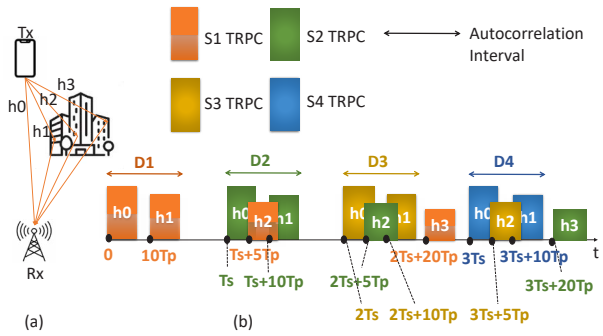

Fig. 2. An example of a TRPC block consisting of four symbols transmitted via a multi-path channel (a) Four-tap example channel (b) Received signal affected by ISI and auto-correlation interval for each symbol

are developed to deal with ISI within the block, while inter-block interference (IBI) is handled by the guard interval.

The rest of the paper is organized as follows. The system model is given in Section II. Section III formulates channel estimation and equalization (CEE). Section IV presents simulation results. Section V draws the conclusions.

II. System Model

The proposed block-based TRPC design is shown in Fig. 1. Transmission time is divided into slots, with the channel assumed stable during each slot. One time slot begins with a pilot block followed by several data blocks, where a block has a guard interval (GI) in the front. Please note that although the block structure looks similar to orthogonal frequency division multiplexing (OFDM), it is time-domain single carrier block transmission. The receiver first removes the guard interval and performs autocorrelation for the symbols in each block. The subsequent ISI processing will be detailed in the next sections. The structure of a single TRPC symbol is described in [4]. A TRPC transmission block is formed by N symbols, each of which has a duration of T_s. The i-th TRPC symbol in a block is composed of N_p pulses, denoted by $p(t)$, with a duration of T_p, i.e.,

$$s_i(t) = \sum_{m=0}^{N_p/2-1} p(t - 2mT_p) + b_i p(t - (2m+1)T_p), \quad (1)$$

with $(i-1)T_s < t < iT_s$. The BPSK modulated data b_i takes values of $+1$ or -1. The pulse cluster of the i-th symbol has a duration of $N_pT_p < T_s$, and the rest of the symbol duration is zero. The transmitted signal of one block is given by

$$s(t) = \sum_{i=0}^{N-1} s_i(t - iT_s). \quad (2)$$

In this paper, the multi-ray THz channel model developed using ray tracing method [15] is adopted, which captures rough surface scattering while considering attenuation due to molecular absorption of the atmosphere. The main advantage of the selected model is that it conserves the energy of the channel impulse response, regardless of the number of launched rays in the ray-tracing simulator, or the size of the tiles for the scattering surface. The received signal is given by

$$r(t) = \sum_{l=0}^{L-1} h_l s(t - \tau_l) \quad (3)$$

where h_l and $\tau_l = k_l T_p$ are the complex gain and the discretized delay of the l-th path, respectively, and k_l is an integer.

III. Channel Estimation And Equalization For Block TRPC In THz Bands

At the receiver, after removing the GI, for each symbol, an autocorrelation decision variable is computed. The autocorrelation for the n-th symbol is given by

$$D_n = \sum_j \int_{(n-1)T_s+T_j^{start}}^{(n-1)T_s+T_j^{end}} r^*(t) r(t - T_p) dt. \quad (4)$$

To simplify, set $T_j^{start} = \tau_j + T_p$ and $T_j^{end} = \tau_j + T_j^I$, where T_j^I is the integration interval for the j-th significant cluster (tap) within the symbol duration T_s. To clearly illustrate the autocorrelation output in a block transmission and the subsequent channel estimation with equalization, we use a simple example of channel realization to show the process. In particular, a TRPC block of four symbols $s_i, i \in \{1, 2, 3, 4\}$ is transmitted through a four-tap channel $h(t)$. Each symbol has $N_p = 8$ pulses. The channel's tap delays are expressed in terms of T_p as follows

$$\tau_0 = 0,\ \tau_1 = 10T_p,\ \tau_2 = T_s + 5T_p,\ \tau_3 = 2T_s + 20T_p, \quad (5)$$

where τ_0 is set to 0 since the first tap delay can always be compensated by proper synchronization. The channel delays are illustrated in Fig. 2. In the autocorrelation step, it is assumed in this example that the integration interval should cover the main taps of the channel and less than symbol duration T_s, which means T_s should be larger than the delay spread of significant paths, i.e., $T_j^{start}, T_j^{end} < T_s$. The case in which the collected energy from delayed copies of the signal spread into subsequent symbols, i.e., $T_j^{start} > T_s$, may be needed if the delays of significant channel taps are larger than T_s. As shown in Fig. 2, the h_3 copy is not collected

in autocorrelation of the first symbol and hence no useful signal energy from this tap is collected. Besides, since h_3 does not collide with the multipath copies of the other symbols, it causes no ISI to other symbols. On the other hand, h_2 path energy is also not collected for the first symbol; however, it creates ISI to the subsequent symbols due to overlapping. Assuming the integration interval that covers all the seven TRPC pulses T_p to $8T_p$, the autocorrelation for the first symbol, ignoring the thermal noise, is given by

$$\begin{aligned} D_1 =& \sum_j \int_{T_j^{start}}^{T_j^{end}} r^*(t) r(t-T_p) dt \\ =& \int_{T_p}^{8T_p} h_0^* s_1^*(t) h_0 s_1(t-T_p) dt + \\ & \int_{\tau_1+T_p}^{\tau_1+8T_p} h_1^* s_1^*(t-\tau_1) h_1 s_1(t-\tau_1-T_p) dt \\ =& (|h_0|^2 + |h_1|^2) E_s b_1 = u_0 b_1, \end{aligned} \tag{6}$$

where $E_s b_1 = \int_{T_p}^{8T_p} s_1^*(t) s_1(t-T_p) dt$ and $u_0 = (|h_0|^2 + |h_1|^2)$. Next, the autocorrelation output for the second symbol is given by (7), where $u_1 b_1$ and I_2 represent adjacent ISI and other partial interference, respectively. Similarly, the value of D_3 and D_4 can be computed while replacing b_2 by b_3 or b_4, and b_1 by b_2 or b_3. The values of $\rho_{21}, \rho_{12}, \zeta_{21}, \zeta_{12}$ also depend on b_1, b_2. For D_3, the values of $\rho_{32}, \rho_{23}, \zeta_{32}, \zeta_{23}$ depend on b_2, b_3. Likewise, in D_4, $\rho_{43}, \rho_{34}, \zeta_{43}, \zeta_{34}$ depend on b_3, b_4. The autocorrelation values can be rewritten as

$$\begin{aligned} D_1 &= u_0 b_1 + I_1, \text{with } I_1 = 0, \\ D_2 &= u_0 b_2 + u_1 b_1 + I_2, \\ D_3 &= u_0 b_3 + u_1 b_2 + I_3, \\ D_4 &= u_0 b_4 + u_1 b_3 + I_4. \end{aligned} \tag{8}$$

If a zero prefix (ZP) is used in front of b_1 of the block, the equations can be given in a matrix form as

$$D = \begin{bmatrix} D_1 \\ D_2 \\ D_3 \\ D_4 \end{bmatrix} = \begin{bmatrix} u_0 & 0 & 0 & 0 \\ u_1 & u_0 & 0 & 0 \\ 0 & u_1 & u_0 & 0 \\ 0 & 0 & u_1 & u_0 \end{bmatrix} \begin{bmatrix} b_1 \\ b_2 \\ b_3 \\ b_4 \end{bmatrix} + \begin{bmatrix} I_1 \\ I_2 \\ I_3 \\ I_4 \end{bmatrix} = U_z b + I. \tag{9}$$

In case of a cyclic prefix (CP), the matrix form is given by

$$D = \begin{bmatrix} D_1 \\ D_2 \\ D_3 \\ D_4 \end{bmatrix} = \begin{bmatrix} u_0 & 0 & 0 & u_1 \\ u_1 & u_0 & 0 & 0 \\ 0 & u_1 & u_0 & 0 \\ 0 & 0 & u_1 & u_0 \end{bmatrix} \begin{bmatrix} b_1 \\ b_2 \\ b_3 \\ b_4 \end{bmatrix} + \begin{bmatrix} I_1 \\ I_2 \\ I_3 \\ I_4 \end{bmatrix} = U_c b + I. \tag{10}$$

The CP/ZP length is determined by the channel root-mean-square delay spread. Then to ensure a desirable CP/ZP overhead rate, the block length is chosen. In the example channel, 4 CP/ZP symbols are necessary and to achieve 25% overhead, the TRPC block length can be 16 symbols. In (10), the noise and interference power are important factors in the autocorrelation process. Therefore, the MMSE CEE is a good fit to balance the trade-off between ISI and noise amplification. Moreover, a larger number of u's can be considered if interference from additional previous symbols is to be included. Using a pilot block P to estimate the equivalent channel u's, the autocorrelation output matrix D_P is given by

$$D_P = PU + I + n, \tag{11}$$

which can be expressed as the following for the described example assuming CP,

$$\begin{bmatrix} D_{P1} \\ D_{P2} \\ \vdots \\ D_{P15} \\ D_{P16} \end{bmatrix} = \begin{bmatrix} P_1 & P_{16} & P_{15} & P_{14} \\ P_2 & P_1 & P_{16} & P_{15} \\ \vdots & \vdots & \vdots & \vdots \\ P_{15} & P_{14} & P_{13} & P_{12} \\ P_{16} & P_{15} & P_{14} & P_{13} \end{bmatrix} \begin{bmatrix} u_0 \\ u_1 \\ u_2 \\ u_3 \end{bmatrix} + \begin{bmatrix} I_1 \\ I_2 \\ \vdots \\ I_{15} \\ I_{16} \end{bmatrix} + n. \tag{12}$$

The goal of the MMSE channel estimation is to find a weight matrix W_{MMSE}^P that minimizes the mean squared error between matrix U and the weighted received signal $W_{MMSE}^P D_P$. The MMSE weight matrix can be computed as

$$W_{MMSE}^P = P^H (P P^H + N_0 Q)^{-1}, \tag{13}$$

where P^H is the Hermitian transpose of P, N_0 is the variance of interference I and noise n , and Q is the identity matrix. The estimated equivalent channel vector $\hat{U}_{MMSE} = \begin{bmatrix} \hat{u}_0 \hat{u}_1 \hat{u}_2 \hat{u}_3 \end{bmatrix}'$ can be obtained by

$$\hat{U}_{MMSE} = W_{MMSE}^P D_P. \tag{14}$$

For data detection, the autocorrelation output matrix D of one data block is written as

$$D = U^b b + I + n \tag{15}$$

where $U^b = \text{circ}(u_0, 0, \ldots, u_3, u_2 u_1)$ assuming the channel u's remain the same in data blocks and the pilot block. The detected transmitted signal is given by

$$\hat{b}_{MMSE} = W_{MMSE}^b D \tag{16}$$

where

$$W_{MMSE}^b = (\hat{U}_{MMSE}^b)^H [\hat{U}_{MMSE}^b (\hat{U}_{MMSE}^b)^H + N_0 Q]^{-1} \tag{17}$$

and $\hat{U}_{MMSE}^b = \text{circ}(\hat{u}_0, 0, \ldots \hat{u}_3, \hat{u}_2 \hat{u}_1)$ is a 16×16 circulant matrix with the estimated equivalent channel coefficients $\hat{u}$'s from (14), given CP is used.

IV. Simulation Results And Discussion

A. Simulation Settings

This section compares the performance of the proposed TRPC block transmission with CEE and the original TRPC [4] in THz channels. The coefficients and time delay of the simulated THz channels at $0.3, 0.7,$ and 0.85 THz are illustrated in Fig. 3. The environment is a small office room with a dimension of $d_1 \times d_2 \times d_3 = 16.75 \times 35.9 \times 3$ m^3 featuring rough plaster or wallpaper walls [15]. The roughness parameters follow coherence length $L = 1.3$ mm, rms hight $\sigma = 0.05$ mm for plaster, and $L = 2.3$ mm, $\sigma = 0.13$ mm

$$
\begin{aligned}
D_2 &= \int_{T_s+\tau_0+T_p}^{T_s+\tau_0+8T_p} \big[h_0 s_2(t-T_s-\tau_0)+h_1 s_2(t-T_s-\tau_1)+h_2 s_1(t-\tau_2)\big]^* \\
&\big[h_0 s_2(t-T_s-\tau_0-T_p)+h_1 s_2(t-T_s-\tau_1-T_p)+h_2 s_1(t-\tau_2-T_p)\big]dt \\
&+ \int_{T_s+\tau_1+T_p}^{T_s+\tau_1+8T_p} \big[h_0 s_2(t-T_s-\tau_0)+h_1 s_2(t-T_s-\tau_1)+h_2 s_1(t-\tau_2)\big]^* \\
&\big[h_0 s_2(t-T_s-\tau_0-T_p)+h_1 s_2(t-T_s-\tau_1-T_p)+h_2 s_1(t-\tau_2-T_p)\big]dt \\
&= \int_{T_p}^{8T_p} |h_0|^2 s_2^*(t)s_2(t-T_p)dt + \int_{T_p}^{8T_p} |h_1|^2 s_2^*(t)s_2(t-T_p)dt \\
&+ \int_{T_p}^{8T_p} \big[h_0^* s_2^*(t)h_2 s_1(t-6T_p)+h_2^* s_1^*(t-5T_p)h_2 s_1(t-6T_p)+h_2^* s_1^*(t-5T_p)h_0 s_2(t-T_p)\big]dt \\
&+ \int_{T_p}^{8T_p} \big[h_1^* s_2^*(t)h_2 s_1(t+5T_p-T_p)+h_2^* s_1^*(t+5T_p)h_2 s_1(t+5T_p-T_p)+h_2^* s_1^*(t+5T_p)h_1 s_2(t-T_p)\big]dt \\
&= (|h_0|^2+|h_1|^2)E_s b_2 + |h_2|^2 pE_s b_1 + h_0^* h_2 \rho_{21} + h_2^* h_0 \rho_{12} + h_1^* h_2 \zeta_{21} + h_2^* h_0 \zeta_{12} = u_0 b_2 + u_1 b_1 + I_2.
\end{aligned}
\tag{7}
$$

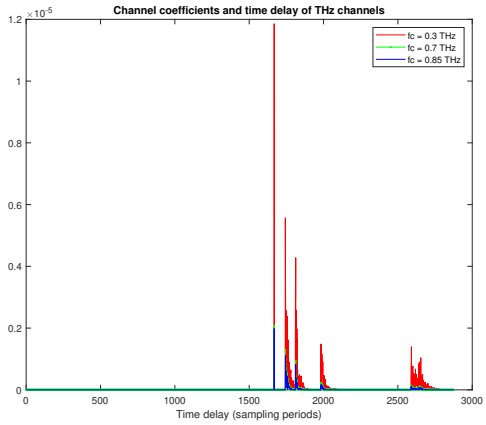

Fig. 3. Channel coefficients and time delay of THz channels used in simulation

TABLE I
SIMULATION PARAMETERS

Parameter	Description
Center frequency f_c	$0.3, 0.7, 0.85$ THz
Bandwidth BW	10 GHz
Pulse duration T_p	0.1 ns
Simulation sampling rate F_s	80 GHz
Channel	Ray-tracing based THz channels with diffused scattering
Channel estimation	MMSE estimated CSI by CN-dedicated pilot signal
Channel equalization	MMSE
Modulation	BPSK
Modulated symbol duration	$115-190$ samples
Block size	16 symbols/block
Prefix length	25% of block length
Channel coding	N/A

for wallpaper [16]. The channel has five clusters, including light-of-sight and reflections from four surrounding walls. Four rough surface areas with dimensions $l_x = l_y = 50L$ centered around the specular reflection point on the four walls are considered. The rough surface is divided into $N \times M = 51 \times 51$ small square tiles, each of which generates a diffuse scattering ray. The transmitter and receiver distance is $d = 6$ m. From Fig. 3, the total path gain decreases as the frequency increases due to the spreading loss. The simulation settings are summarized in Table I. Note that the simulation sampling rate 80 GHz is 8 times oversampling to a single pulse in the pulse cluster of bandwidth 10 GHz, simply to represent the analog waveform of a single pluse in Matlab simulation. The receiver's actual analog-to-digital rate is the same as the inverse of the symbol duration. That is, the decision variable at the autocorrelation analog output is sampled at the symbol rate, much lower than the pulse bandwidth 10 GHz. The symbol duration is expressed in terms of the number of samples with 80 GHz simulation sampling rate in the paper.

One TRPC symbol consists of eight pulses with a duration of 0.8 ns (64 samples) followed by a blank duration which can be expressed by zero samples. The length of the blank duration is adjusted to change the symbol duration. The choice of prefix length is determined by the channel delay spread. For the THz channel simulated, 4 symbol long prefix is sufficient given the range of symbol duration studied. Once the prefix length is chosen, the pilot and data block length is four times of prefix length, considering a prefix overhead of 25%. Fig. 1 depicts the length of one data and one pilot block in terms of samples. A time slot starts with a pilot block, followed by multiple data blocks, given the stable channel in the time slot. In the TRPC demodulation process, the autocorrelation integration intervals are decided based on the significant channel segments, whose amplitudes are higher than a set threshold. The autocorrelation length does not exceed the symbol duration.

The pilot signal is transmitted with 10 dB higher power to improve the accuracy of estimated u values. The MMSE CEE algorithms with two and four u values are tested for equivalent channel estimation with both ZP and CP. For channel equalization, the value of noise and interference variance N_0 in (11) and (15) is set to 0.5. The simple BPSK modulation scheme is adopted. The performance of the proposed scheme varies depending on the center frequencies, channels, symbol duration, and pilot patterns. Four pilot patterns, selected heuristically based on the arrangement of 1s and the number of subsequent 0s, are given in Table II. The optimal pilot patterns for different symbol duration, data rate, and carrier frequencies are summarized in Table III. A detailed study of optimal pilot patterns will be addressed in future work.

TABLE II
PILOT PATTERNS

No.	Pilot pattern	No.	Pilot pattern
1	0111101111101010	2	0111101111011111
3	0111101111100000	4	0111101110010010

TABLE III
SELECTED PILOT PATTERNS FOR DIFFERENT SYMBOL DURATIONS, CENTER FREQUENCIES, AND DATA RATE VALUES

Data rate (Mbps)	Symbol duration (samples)	f_c (THz)	Selected pilot pattern
420	190	0.3/0.7/0.85	4/1/2
520	153	0.3/0.7/0.85	3/3/3
600	133	0.3/0.7/0.85	3/4/4
630	126	0.3/0.7/0.85	3/4/3
690	115	0.3/0.7/0.85	3/3/3

B. Simulation Results And Discussion

Next, the bit error rates versus the received SNR of the selected schemes in the THz channels with various symbol durations are shown in Figs. 4-8. To clearly benchmark the benefits of prefixes and CEE algorithms, phase noise will be temporarily disregarded in this section. The overall trend indicates that as the symbol duration decreases, the performance of all schemes degrades due to higher ISI. Some observations can be drawn as follows. First, the effectiveness of using prefixes alone without CEE algorithms is limited, particularly in the case of CP. Indeed, block TRPC with CP only usually has the same performance as the original TRPC, as shown in most of the figures. It is because although prefixes can help reduce IBI from the preceding block on the succeeding block, the CP itself introduces interference to the subsequent one. Block TRPC with ZP, on the other hand, offers a slight improvement in BER over the original TRPC, as ZP does not introduce interference to the later symbols. This trend, shown in Figs. 4(a), 5, and 6(a), indicates that ZP alone is effective at shorter symbol durations, where IBI dominates over ISI, particularly in scenarios with higher channel gains at 300 GHz.

Secondly, including CEE algorithms along with the prefixes, the impact of THz channels is markedly reduced, especially at 300 GHz. Indeed, as illustrated in Figs. 4(a)-8(a), for all symbol duration values at 300 GHz, the block TRPC with 'CEE and prefixes' schemes outperform the original TRPC and block TRPC with 'prefixes only' by a large margin. For $f_c = 0.7$ and 0.85 THz, the proposed algorithms demonstrate higher performance gains as the symbol duration values get shorter. Specifically, the performance gain becomes noticeable as the symbol duration decreases from 153 (Figs. 5(b),(c)) to 115 (Figs. 8(b),(c)). In contrast, at longer symbol durations, such as 190 (Figs. 4(b),(c)), the effectiveness of 'CEE and prefixes' is less pronounced. This difference is expected, as the ISI is less severe at the longer symbol durations due to the smaller channel delay spread when $f_c = 0.7$ and 0.85 THz. However, at 300 GHz, as shown in Fig. 3, the channel has higher coefficients at long delays, which gives rise to harsh ISI even at long symbol duration rates. As can be seen in Figs. 4(b), 5-7, among the transmission schemes

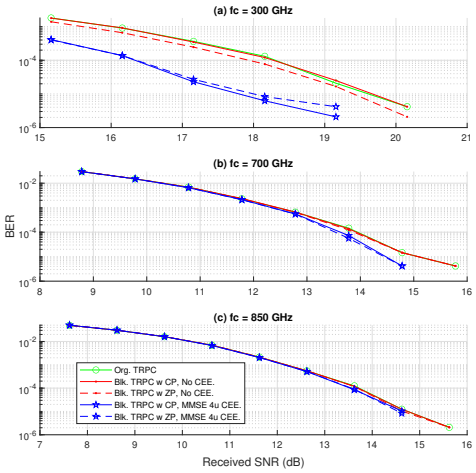

Fig. 4. BER of Original TRPC vs Block TRPC with prefixes and CEE; BPSK; Symbol Duration = 190 samples; fc = 0.3, 0.7, 0.85 THz.

employing both CEE and prefixes, the MMSE 4u, generally achieves lower BER, benefiting from more precise u-value estimation. The only symbol duration, in which MMSE 2u provides a better performance, is 115 as shown in Fig. 8(a). Additionally, CP tends to offer slightly better performance than ZP, owing to its cyclic structure. However, these trends are not always consistent, as the performance may vary with center frequencies, channel conditions, symbol durations, and pilot patterns. The impact of phase noise can be mitigated by the autocorrelation in (4). Moreover, the complexity of Block TRPC is expected to be lower than that of other single-carrier waveforms, such as DFT-s-OFDM and SC- FDE, due to the additional DFT/IDFT blocks required in their processing chains. An in-depth analysis of phase noise effects and complexity will be presented in future work.

V. CONCLUSIONS

The proposed Block TRPC achieves higher data rates and enhances error performance compared to the original TRPC by incorporating prefixes and utilizing MMSE-based channel estimation and equalization. Additionally, the block structure would facilitate multiple access through TDMA. These advantages position block TRPC as a promising waveform for future THz communication systems. The performance of Block TRPC and other single-carrier waveforms under the influence of severe THz channels and phase noise will be considered in a future work.

ACKNOWLEDGMENT

This research is supported by Huawei Technologies Canada.

REFERENCES

[1] Z. Chen, C. Han, Y. Wu, L. Li, C. Huang, Z. Zhang, G. Wang, and W. Tong, "Terahertz wireless communications for 2030 and beyond: A cutting-edge frontier," *IEEE Communications Magazine*, vol. 59, no. 11, pp. 66–72, 2021.

[2] K. Witrisal, G. Leus, G. J. Janssen, M. Pausini, F. Trösch, T. Zasowski, and J. Romme, "Noncoherent ultra-wideband systems," *IEEE Signal Processing Magazine*, vol. 26, no. 4, pp. 48–66, 2009.

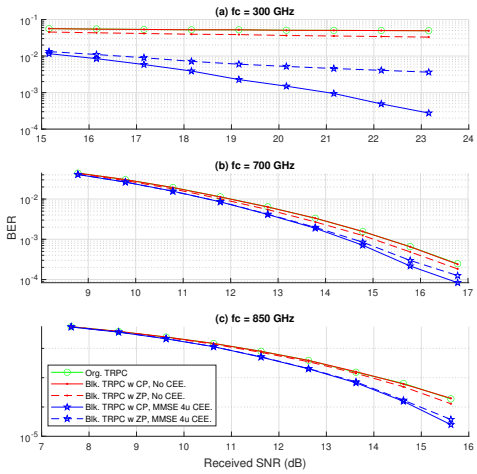

Fig. 5. BER of Original TRPC vs Block TRPC with prefixes and CEE; BPSK; Symbol Duration = 153 samples; fc = 0.3, 0.7, 0.85 THz.

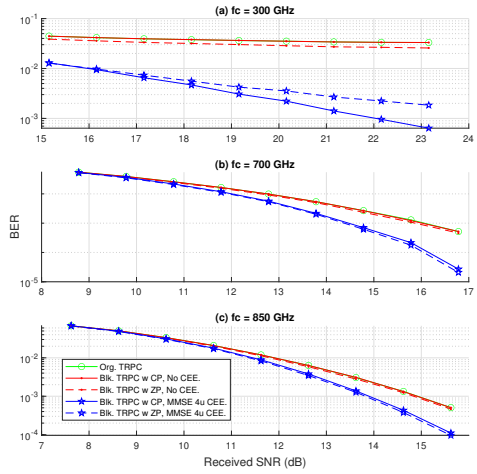

Fig. 6. BER of Original TRPC vs Block TRPC with prefixes and CEE; BPSK; Symbol Duration = 133 samples; fc = 0.3, 0.7, 0.85 THz.

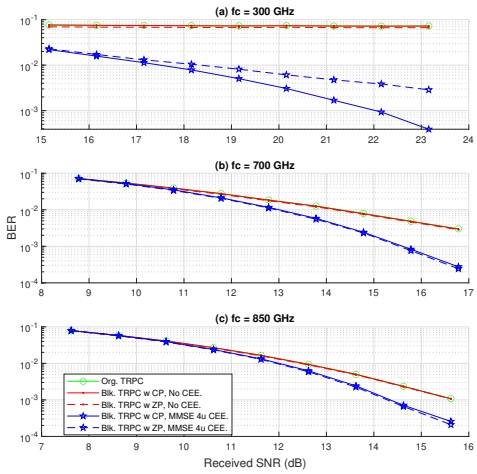

Fig. 7. BER of Original TRPC vs Block TRPC with prefixes and CEE; BPSK; Symbol Duration = 126 samples; fc = 0.3, 0.7, 0.85 THz.

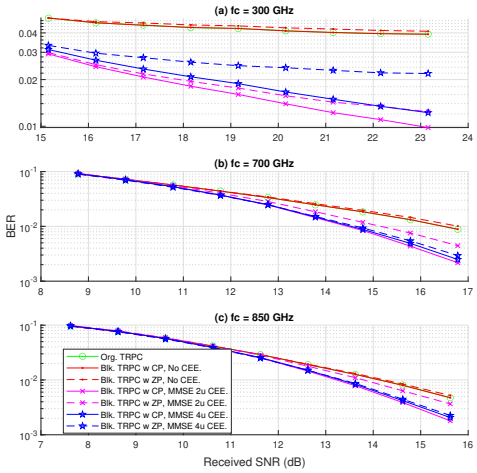

Fig. 8. BER of Original TRPC vs Block TRPC with prefixes and CEE; BPSK; Symbol Duration = 115 samples; fc = 0.3, 0.7, 0.85 THz.

[3] V. Niemelä, J. Haapola, M. Hämäläinen, and J. Iinatti, "An ultra wideband survey: Global regulations and impulse radio research based on standards," *IEEE Communications Surveys & Tutorials*, vol. 19, no. 2, pp. 874–890, 2016.

[4] X. Dong, L. Jin, and P. Orlik, "A new transmitted reference pulse cluster system for uwb communications," *IEEE Transactions on Vehicular Technology*, vol. 57, no. 5, pp. 3217–3224, 2008.

[5] I. Guvenc, Z. Sahinoglu, and P. V. Orlik, "Toa estimation for ir-uwb systems with different transceiver types," *IEEE Transactions on Microwave Theory and Techniques*, vol. 54, no. 4, pp. 1876–1886, 2006.

[6] Z. Liang, X. Dong, X. Yang, and H. Song, "Digital weighted autocorrelation receiver using channel characteristic sequences for transmitted reference uwb communication systems," in *2016 IEEE Wireless Communications and Networking Conference*. IEEE, 2016, pp. 1–5.

[7] S. Nagaraj and F. G. Rassam, "Improved noncoherent uwb receiver for implantable biomedical devices," *IEEE Transactions on Biomedical Engineering*, vol. 63, no. 10, pp. 2220–2225, 2015.

[8] T. P. Do, S. R. Lee, and Y. H. Kim, "An enhanced frequency-shifted reference ultrawideband scheme for low data rate applications," in *The Sixth International Workshop on Signal Design and Its Applications in Communications*. IEEE, 2013, pp. 16–19.

[9] Y. Dai and X. Dong, "Hybrid ppm-bpsk for transmitted reference pulse cluster systems in uwb and 60-ghz channels," *IEEE Wireless Communications Letters*, vol. 3, no. 6, pp. 657–660, 2014.

[10] Z. Liang, G. Zhang, X. Dong, and Y. Huo, "Design and analysis of passband transmitted reference pulse cluster uwb systems in the presence of phase noise," *IEEE Access*, vol. 6, pp. 14 954–14 965, 2018.

[11] Y. Jin, J. Sun, L. Dai, P. Cai, K. S. Kwak, and S.-J. Yoo, "A solution to the non-ideal delay line problem in transmitted reference pulse cluster schemes for uwb communications," *IEEE Internet of Things Journal*, vol. 10, no. 2, pp. 1162–1170, 2022.

[12] Y. Jin, J. Sun, C. Chen, W. Chen, and Y. Bai, "An energy efficient on-off keying transmitted reference pulse cluster system for uwb communications," *IEEE Transactions on Vehicular Technology*, vol. 72, no. 8, pp. 10 440–10 447, 2023.

[13] Y. Jin and X. Kuang, "An energy-efficient weighting strategy for various trpc-uwb communication systems," *IEEE Internet of Things Journal*, 2024.

[14] S. Sharma, V. Bhatia, and A. Gupta, "Joint symbol and toa estimation for iterative transmitted reference pulse cluster uwb system," *IEEE Systems Journal*, vol. 13, no. 3, pp. 2629–2640, 2018.

[15] A. M. Khamse, X. Dong, and N. Ferdinand, "The scattering channel model for terahertz wireless communications," *IEEE Open Journal of the Communications Society*, vol. 4, pp. 810–822, 2023.

[16] C. Jansen, S. Priebe, C. Moller, M. Jacob, H. Dierke, M. Koch, and T. Kurner, "Diffuse scattering from rough surfaces in thz communication channels," *IEEE Transactions on Terahertz Science and Technology*, vol. 1, no. 2, pp. 462–472, 2011.